ELSEVIER

Materials Science and Engineering A301 (2001) 80–89

MATERIALS SCIENCE & ENGINEERING A

www.elsevier.com/locate/msea

Fabrication and evaluation of plasma sprayed nanostructured alumina–titania coatings with superior properties

E.H. Jordan [a], M. Gell [b], Y.H. Sohn [b], D. Goberman [b], L. Shaw [b,*], S. Jiang [c], M. Wang [c], T.D. Xiao [c], Y. Wang [c], P. Strutt [c]

[a] *Department of Mechanical Engineering, Institute of Materials Science, University of Connecticut, Storra, CT 06269-3136, USA*
[b] *Department of Metallurgy and Materials Engineering, Institute of Materials Science, University of Connecticut, Storra, CT 06269-3136, USA*
[c] *Inframat Corporation, 20 Washington Avenue, North Haven, CT 06473, USA*

Received 5 January 2000; received in revised form 31 March 2000

Abstract

Reconstituted nanostructured powders were plasma sprayed using various processing conditions to produce nanostructured alumina–titania coatings. Properties of the nanostructured coatings were related to processing conditions through a critical plasma spray parameter (CPSP) that in turn, can be related to the amount of unmelted powder incorporated into the final coating. Those coatings that retain a significant amount of unmelted powder show optimum microstructure and properties. Selected physical and mechanical properties were evaluated by X-ray diffraction (XRD), optical and electron microscopy, quantitative image analysis and mechanical testing. Constituent phases and the microstructure of the reconstituted particles and plasma sprayed coatings were examined with the aid of quantitative image analysis as a function of processing conditions. Mechanical properties including hardness, indentation crack growth resistance, adhesion strength, spallation resistance during bend- and cup-tests, abrasive wear resistance and sliding wear resistance were also evaluated. These properties were compared with a commercial plasma sprayed alumina–titania coating with similar composition. Superior properties were demonstrated for nanostructured alumina–titania coatings plasma sprayed at optimum processing conditions.

Keywords: Alumina–titania coatings; Thermal spray; Nanomaterials

1. Introduction

Nanostructured ceramic coatings produced by plasma spray processes are being developed for a wide variety of applications that require resistance to wear, erosion, cracking and spallation [1]. Attractive properties associated with a nanostructure (in general referring to grain size smaller than 100 nm) have been documented for bulk materials [1–8]. It is anticipated that, if properly deposited, nanostructured ceramic coatings could also provide improved properties for variety of applications, including wear resistant [9,10] and thermal barrier coatings [11,12]. Thermal spray techniques are often used to deposit thick oxide coatings, and experimental examination of phase constituents, microstructures and mechanical properties with respect to processing conditions have been extensively carried out and reviewed [13–19]. This is the first paper that deals with similar studies for nanostructured coatings.

2. Experimental procedure

The nanostructured Al_2O_3 and TiO_2 powders employed in this study were obtained from Nanophase Technology Corporation™, Burr Ridge, IL. The powders have a mean diameter of 50 and 70 nm, respectively. These powders were blended to produce a powder mixture with composition equivalent to commercially available Metco-130 (Al_2O_3-13wt.%TiO_2). In addition, small amounts of nanostructured oxide pow-

* Corresponding author. Tel.: +1-860-4864620; fax: +1-860-4864745.
E-mail address: lshaw@mail.ims.uconn.edu (L. Shaw).

0921-5093/01/$ - see front matter
PII: S0921-5093(00)01382-4

Table 1
Specimen designation for plasma sprayed alumina–titania coatings and the corresponding CPSP values

CPSP	Commercial coating Metco-130	Nano-alumina–titania	Modified nano-alumina–titania[a]
270	–	S270	–
300	C300	S300	M300
325	C325	S325	M325
350	–	–	M350
390	–	–	M390
410	C410	–	M410

[a] Modified with small amounts of other additives.

ders were added during mixing for a modified nanostructured powder. The mixed powders were then reconstituted to form micrometer-size agglomerates (40–70 μm) that are large enough to be used commercial powder feeders. The process of reconstitution consists of spray drying a slurry containing nano-alumina and nano-titania particles and subsequent heat treatment at high temperature (800–1200°C). Plasma reprocessing of the powders was carried out for the modified powders. Characterization of the reconstituted agglomerates, as well as Metco-130 powders, were carried out by X-ray diffraction (XRD) and electron microscopy for phase identification and examination of agglomerate size, shape, morphology and microstructure.

Plasma spray of the reconstituted agglomerates and Metco-130 powders was carried out with a Metco 9 MB plasma torch and GH nozzle. The coatings were deposited up to 300 μm thick on mild carbon steel substrates of various geometries specifically designed for specific mechanical property tests. The plasma spray of oxide coatings in this study was carried out as a function of a critical plasma spray parameter (CPSP) defined as [9]:

$$\text{CPSP} = \frac{\text{Voltage} \times \text{Current}}{\text{Primary Gas (Ar) Flow Rate}} \quad (1)$$

Other processing variables such as carrier gas flow rate, spray distance, flow rate ratio of Argon to H_2, powder feed rate, gun speed, etc., were held constant in this study. Under these controlled processing conditions, CPSP can be directly related to the temperature of the plasma and/or the particles [20]. The alumina–titania coatings deposited by plasma spraying at various CPSP values are summarized in Table 1.

For each specific CPSP condition, a total of 20 specimens were plasma sprayed concurrently using an apparatus that held all 20 mild steel substrates (approximately 2 mm in thickness). Among these 20 specimens, four coupons (2.54 cm in diameter) were coated for modified ASTM-C633-79 direct pull-test [21], four coupons (2.54 cm in diameter) for abrasive wear test, four plates (5 × 5 cm) for cup test, four plates (6 × 5 cm) for bend test and four plates (5 × 5 cm) for sliding wear test. Schematic illustrations of the cup test and the bend test are presented in Fig. 1 and the detailed description of the direct-pull test, abrasive wear test and sliding wear test are given elsewhere [9,10,21]. Also, microhardness and indentation crack growth resistance of the coatings were measured using Vickers indentation technique (HV_{300} and HV_{3000}, respectively) and the amount of porosity in the coatings were estimated from electron micrographs by quantitative image analysis. In addition, constituent phases were characterized by XRD and an estimate of the volume fraction of microstructural features that developed during the plasma spray was performed using quantitative image analysis.

3. Experimental results

3.1. Constituent phases and microstructure of reconstituted agglomerates

Fig. 2 shows the XRD patterns from the Metco-130 powders, nano-alumina–titania and modified nano-aluminia–titania agglomerates. While the Metco-130 pow-

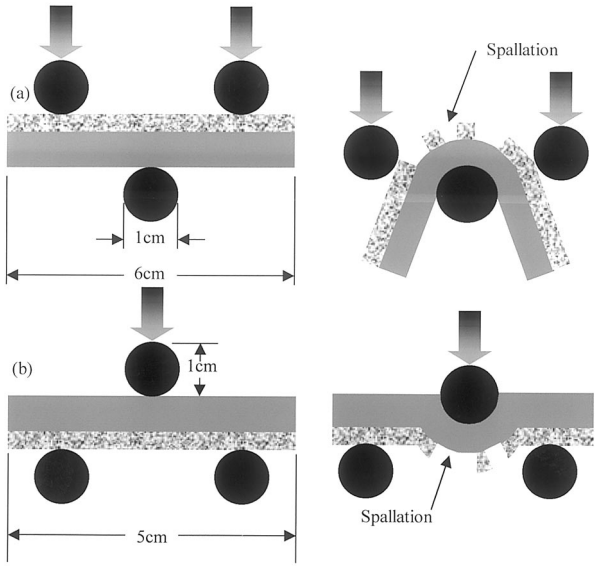

Fig. 1. Schematic illustrations for (a) bend and (b) cup tests carried out for plasma sprayed alumina–titania coatings.

Table 2
Constituent phases of powders/agglomerates prior to plasma spray

Starting powder/agglomerate	Al_2O_3	TiO_2	Others
Commercial coating (Metco-130)	γ	Anatase	–
Nano-alumina–titania	α	Rutile	–
Modified nano-alumina–titania[a]	γ	Anatase	Other oxide phases

[a] Modified with small amounts of other additives.

ders consisted of α-Al_2O_3 and anatase–TiO_2, nano-alumina–titania agglomerates consisted of α-Al_2O_3 and rutile–TiO_2. The modified nano-alumina–titania agglomerates consisted of α-Al_2O_3 and anatase–TiO_2. Additional diffraction peaks from additional phases were observed for modified agglomerates as shown in Fig. 2. The results are summarised in Table 2. Previous work, using XRD [9], has demonstrated that the grain size of α-Al_2O_3 and anatase–TiO_2 is smaller than 100 nm while electron microscopy showed that the grain size of rutile–TiO_2 is smaller than 1000 nm.

The microstructure of the starting powder/agglomerates was studied by using both optical and electron microscopy. Cross-sectional backscattered electron micrographs of Metco-130 and modified nano-alumina–titania coatings after plasma reprocessing are presented in Fig. 3. Based on Saltykov analysis [22] of cross-sectional photomicrographs, the mean particle size was estimated to be 40–70 μm. The reconstituted

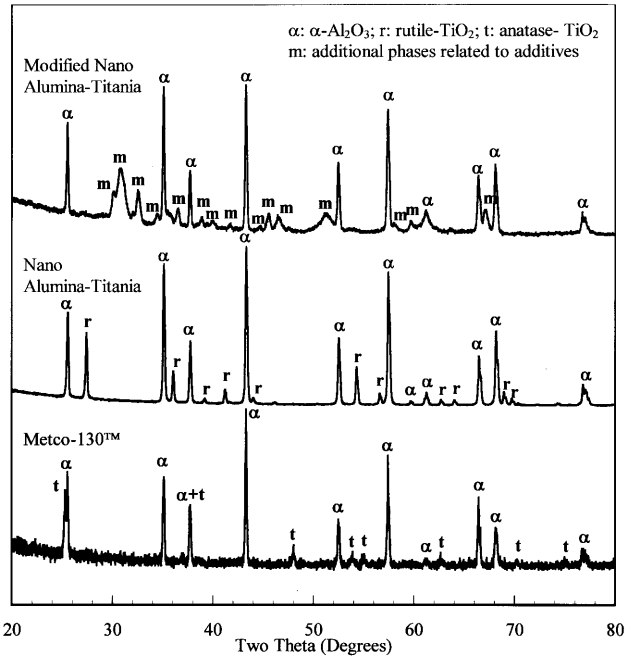

Fig. 2. XRD patterns obtained from Metco-130 powders and reconstituted alumina–titania powders with/without additives.

agglomerates have a spherical morphology, while the Metco-130 powders have an irregular shape. The compositional contrast from backscattered electron micrographs illustrates that the distribution of Al_2O_3 (dark) and TiO_2 (light) is significantly different for Metco-130 powders and modified nano-agglomerates. Typical energy dispersive spectra (EDS) from the dark phase show the presence of Al and the light phase reveals the presence of Ti and Al. With the understanding that the resolution of the EDS is of the order of a micrometer and extraneous signals do contribute to the analysis, it can be concluded that the distribution of the two phases is much finer for nanostructured agglomerates (Fig. 3b).

3.2. Constituent phases and microstructure of plasma sprayed coatings

XRD patterns from all plasma sprayed coatings consist of α- and γ-Al_2O_3; peaks from the TiO_2 phase were not observed. The actual crystal structure regarding γ-Al_2O_3 phase, which may contain Ti ions substitutionally, is presented in Section 4. The relative integrated intensities of the α- and γ-Al_2O_3 peaks (K_α radiation) were calculated and examined as a function of critical plasma spray parameter. The XRD patterns, near the (113) α-Al_2O_3 and (400) γ-Al_2O_3 for modified nano-alumina–titania coatings, shown in Fig. 4, demonstrate that the relative integrated intensity of these peaks depends on the CPSP. Such an observation was examined quantitatively by plotting the ratio of relative integrated intensity, ($E_{K_\alpha}^{\alpha\text{-}Al_2O_3}/E_{K_\alpha}^{\gamma\text{-}Al_2O_3}$) as a function of CPSP as shown in Fig. 5. The ratio ($E_{K_\alpha}^{\alpha\text{-}Al_2O_3}/E_{K_\alpha}^{\gamma\text{-}Al_2O_3}$) increases with a decrease in CPSP for nano- and modified nano-alumina–titania coatings. However, for Metco-130 coatings, such a variation was not observed because these coatings consist mainly of γ-Al_2O_3, independent of CPSP.

A typical microstructure of a plasma sprayed nanostructured alumina–titania coating is presented in Fig. 6. The contrast of the photomicrographs in Fig. 6 originates from electron-charging during secondary electron imaging and was found to be the opposite of the compositional contrast in backscattered electron images. The coating consists of two distinctive microstructures, identified by a fully-melted (FM) region, where columnar grains within lamellar splats are observed, and a partially-melted (PM) region, where some microstructural features of the original particles are observed. These microstructural features include sintered Al_2O_3 particles embedded in a matrix of Al_2O_3–TiO_2 matrix. In general, the shape of the FM region is found to be lamellar, while that of the PM region is non-uniform, ranging from sphere

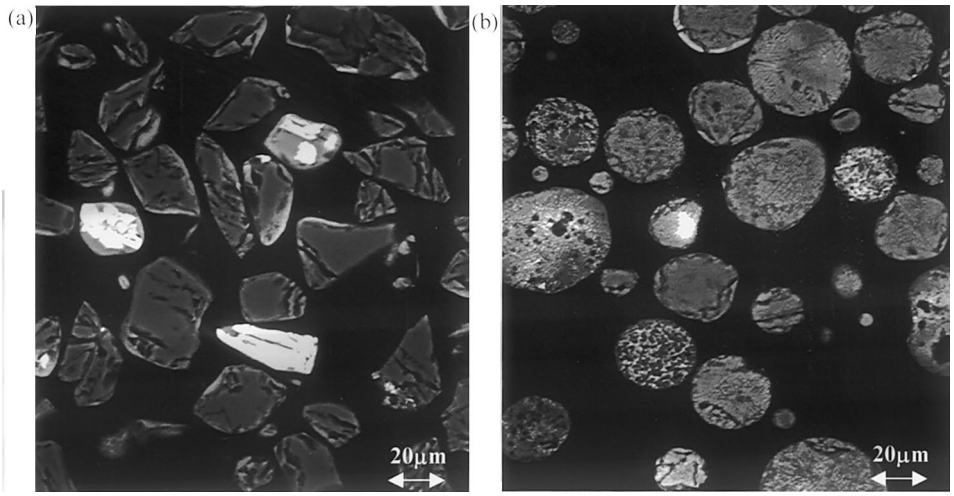

Fig. 3. Backscattered electron micrographs of (a) Metco-130 and (b) modified nano-alumina–titania powders prior to plasma spray.

to lamellae. In Fig. 6d, the lighter phase corresponds to an Al_2O_3 phase and the darker phase corresponds to a Ti-containing Al_2O_3 phase, based on the EDS analysis. From the microstructure of FM and PM regions, it can be inferred that the FM regions consist of splat quenched γ-Al_2O_3 phase and the PM regions consist of sintered α-Al_2O_3 particles, embedded in a matrix of γ-Al_2O_3 that forms from melting and solidification.

Quantitative determination of grain size by XRD cannot be carried out for the plasma sprayed coatings because the presence of non-uniform residual stresses may interfere with the measurement. However, Fig. 6c shows that the splat-quenched FM region contains nano- and submicron-sized columnar grains. Also, the size of the α-Al_2O_3 particles, embedded in the PM region as a result of incomplete melting of the starting agglomerate in the coatings, ranges from 100 to 2000 nm, as shown in Fig. 6d.

The contrast brought out by charging during secondary electron imaging, such as shown in Fig. 6a, has been examined quantitatively by automated image analysis as a function of CPSP. The PM regions appear brighter in the secondary electron images and consist of microstructural features that are retained from the original particles prior to plasma spray. The fraction of the coating microstructure, represented by PM, evaluated by quantitative image analysis as a function of CPSP, is presented in Fig. 7. An increase in the fraction of PM region is observed with a decrease in the CPSP, which can be related to the temperature of the plasma torch and/or particle temperature [20]. Complete melting and a splat-quenched microstructure were observed for Metco-130 coatings plasma sprayed at various CPSP. This result is consistent with the fact that Metco-130 coatings consist primarily of γ-Al_2O_3 independent of CPSP.

3.3. Properties of plasma sprayed coatings

Physical and mechanical properties, including density, hardness, indentation crack growth resistance, adhesive strength, spallation resistance in bend and cup-tests, and resistance to abrasive and sliding wear, of the plasma sprayed coatings were evaluated. These properties were also examined as a function of CPSP and compared with the Metco-130 coatings.

Based on quantitative image analysis, the amount of porosity was evaluated for three coating systems as a function of CPSP, as shown in Fig. 8. A decrease in porosity was observed for both nanostructured and modified-nanostructured alumina–titania coatings with an increase in the CPSP. No variation was observed for Metco-130.

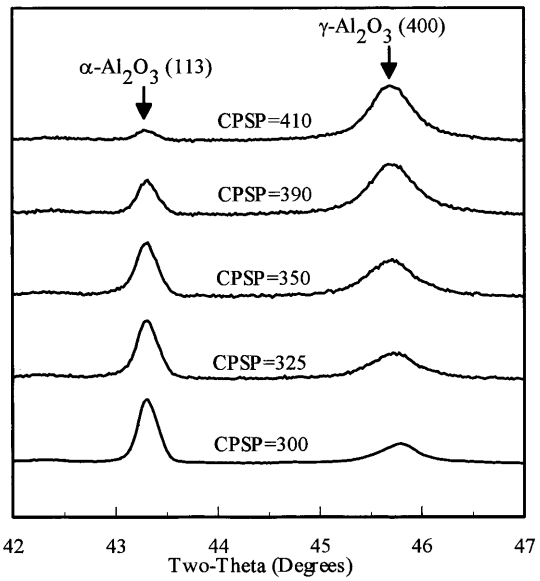

Fig. 4. XRD patterns from (113) α-Al_2O_3 and (400) γ-Al_2O_3 peaks for modified nano-alumina–titania coatings. The relative integrated intensity for these peaks are observed to vary as a function of CPSP.

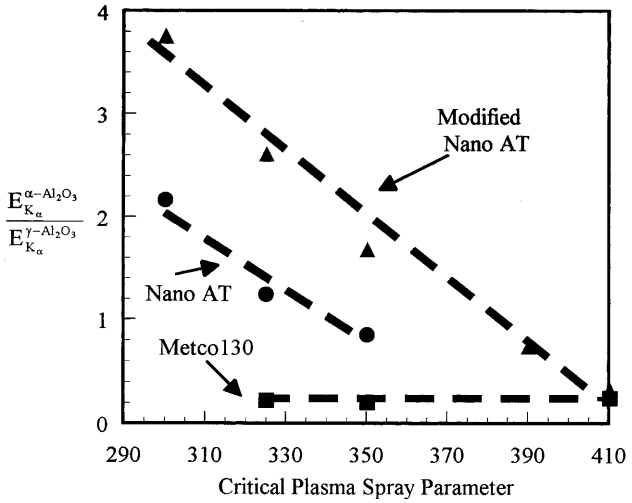

Fig. 5. Ratio of relative integrated intensity of (113) α-Al_2O_3 and (400) γ-Al_2O_3 peaks, ($E^{\alpha\text{-}Al_2O_3}_{K_\alpha}/E^{\gamma\text{-}Al_2O_3}_{K_\alpha}$) calculated from XRD patterns as a function of CPSP.

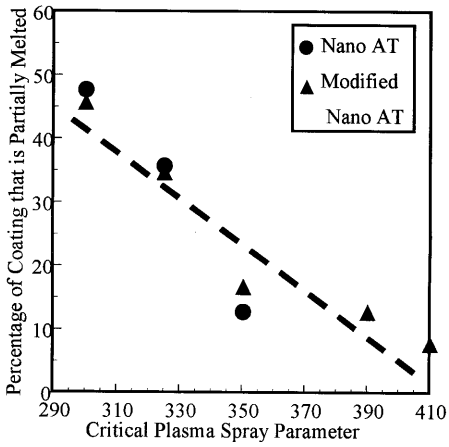

Fig. 7. Percentage of coating that is PM, determined by quantitative image analysis as a function of CPSP.

In Fig. 9, the indentation hardness (HV_{300}) for the three coatings as a function of CPSP is presented. While no variation was observed for Metco-130 coatings, an increase in hardness was observed for nanostructured coatings.

Indentation crack growth resistance of the coatings was also estimated by measuring the length of the two horizontal cracks originating from the corners of the Vickers indentation. A maximum value in the indentation crack growth resistance was observed for nanostructured alumina–titania coatings at an intermediate CPSP (≈ 350) as shown in Fig. 10. The indentation

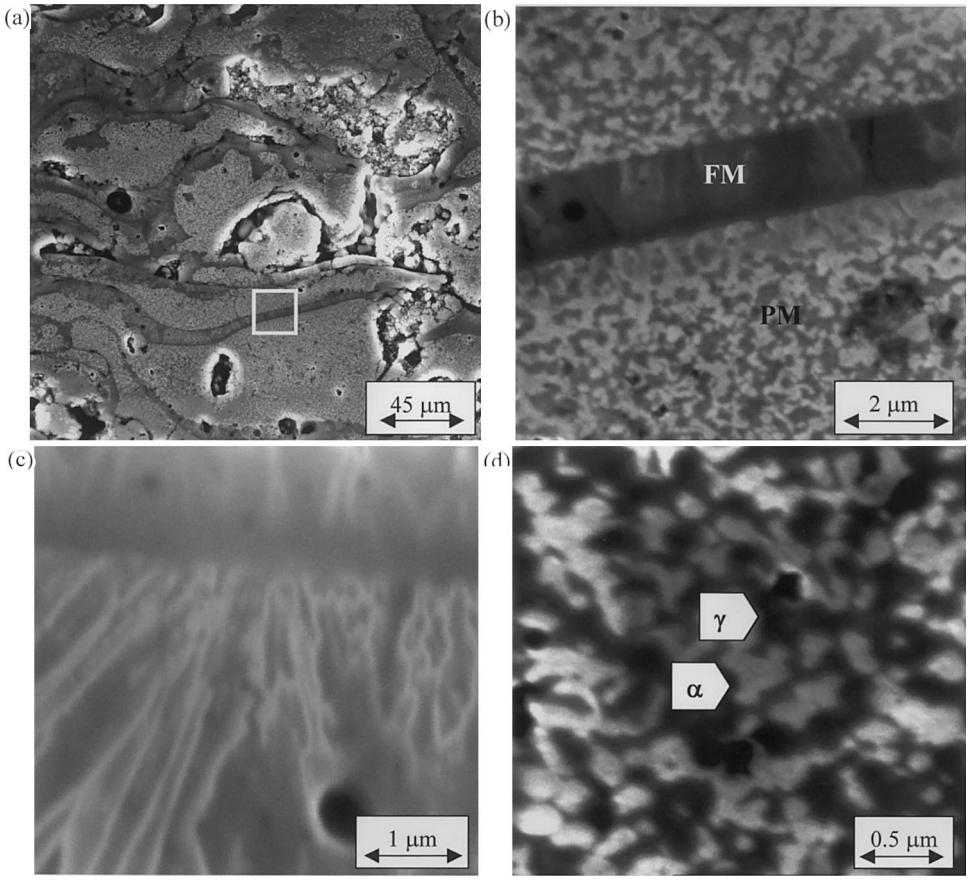

Fig. 6. Secondary electron photomicrographs from plasma sprayed (CPSP = 270) nanostructured alumina–titania coatings. (a) Nanostructured coating consists of two regions identified by (b) FM and PM region. Microstructure in the FM region consists of (c) splat quenched lamellar with columnar grains and the microstructure in the PM region exhibits (d) α-Al_2O_3 nano-particles embedded within γ-Al_2O_3 matrix.

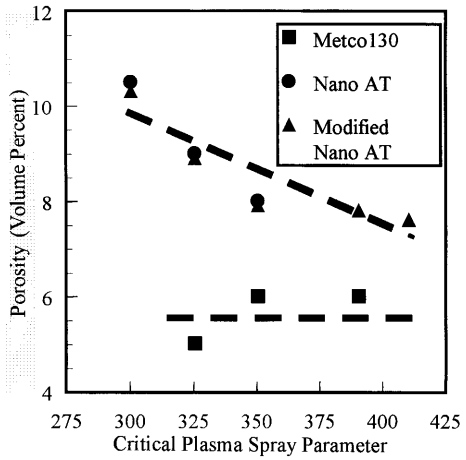

Fig. 8. Percentage of porosity, determined by quantitative image analysis as a function of CPSP.

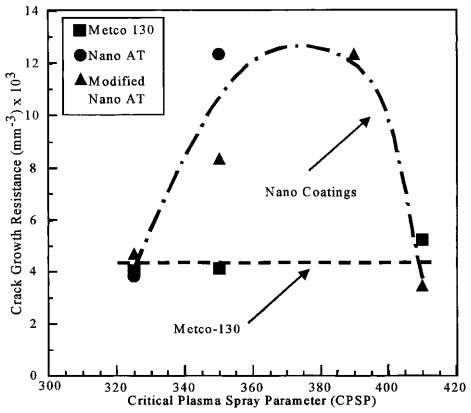

Fig. 10. Indentation crack resistance of plasma sprayed alumina–titania coatings as a function of CPSP.

crack growth resistance of the Metco-130 coatings remain the same as a function of CPSP.

Alumina–titania coatings, plasma sprayed on plate (6×5 cm) substrates, were subjected to bend and cup test, as schematically illustrated in Fig. 1. For each coating type and CPSP, four specimens were tested. Based on visual inspection, the coatings in the bend test were categorized into three groups, (a) complete failure; (b) partial failure and (c) pass. Representative photographs of these results are presented in Fig. 11. Significant spallation, identified as complete failure, was observed for all Metco-130 coatings. However, for nanostructured alumina–titania coatings, partial failure and pass were observed as reported in Table 3. The nanostructured coatings were resistant to bend-failure at lower CPSP.

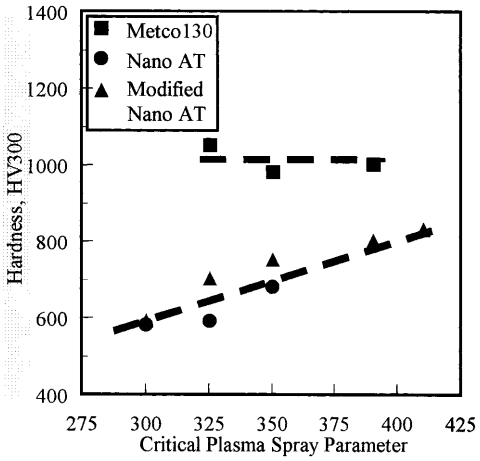

Fig. 9. Hardness (HV_{300}) measured on plasma sprayed alumina–titania coatings as a function of CPSP.

The coatings exhibited similar behavior in cup-tests. While Metco-130 coatings exhibited significant cracking and spallation as shown in Fig. 12a, only minimum spallation was observed without cracking for nanostructure alumina–titania coatings as shown in Fig. 12b.

Adhesive strength of the coatings was measured using the modified ASTM direct-pull test [21]. Significant improvement (>2 X) was observed for nanostructured coatings deposited at selected CPSP's compared with Metco-130 deposited according to manufacturer's recommendation, e.g. CPSP = 410, as shown in Fig. 13. The value of the adhesion strength for the Metco-130 agreed with that specified by the manufacturer [23].

Improvements in the abrasive wear resistance were also observed for nanostructured coatings deposited at selected CPSP's as shown in Fig. 14. Such findings are consistent with previous results where the corresponding wear mechanisms were proposed [10]. Improvement in sliding wear resistance was also observed for nanostructured coatings; consistent with previous results [9]. Details of the results and the associated mechanism related to the improved sliding wear resistance of the nanostructured coatings are currently under investigation.

Typical results from a 'scratch-test' using a diamond indentor are presented in Fig. 15. For nanostructured coatings, the wear track has a small width and a minimum extrusion of materials. For Metco-130 coatings, the wear track is wider with more debris. These observations from 'scratch-tests' support the improved abrasive and sliding wear resistance realized by nanostructured alumina–titania coatings deposited by plasma spray process at appropriate CPSP.

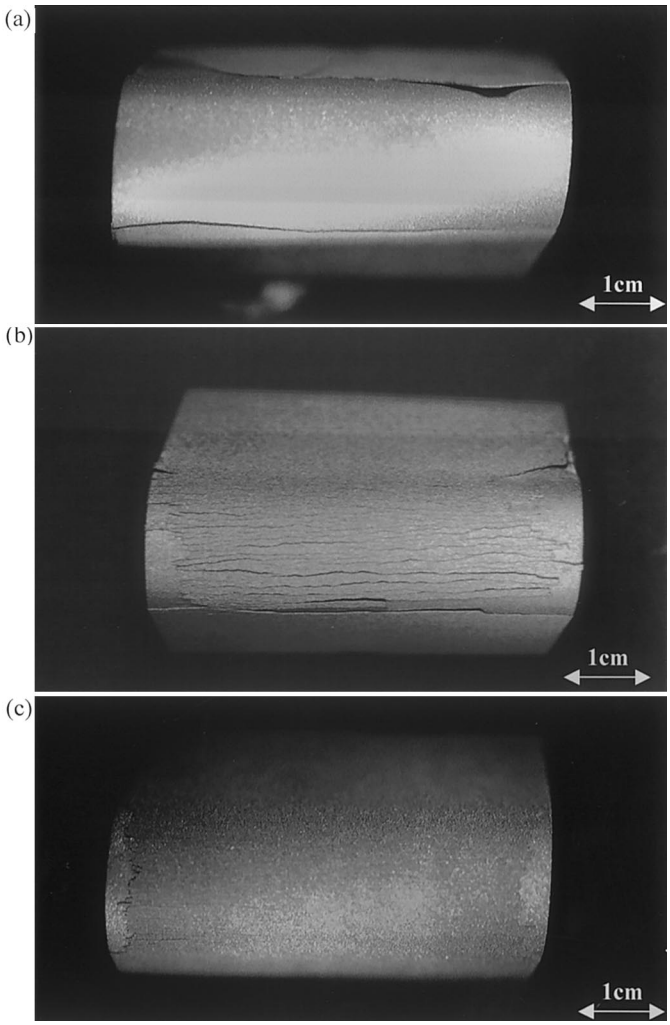

Fig. 11. Photographs of representative results from bend tests. (a) Complete failure, (b) partial failure and (c) pass. Complete failure was observed for all Metco-130 coatings while partial/no failure was observed for nanostructured alumina–titania coatings.

4. Discussion

4.1. Phase constituents, microstructure, and critical plasma spray parameter

The phase constituents of the reconstituted nanostructured agglomerates can be related to processing conditions. For nanostructured Al_2O_3-13wt.%TiO_2, heat treatment at high temperature (800–1200°C) produces the equilibrium phase for both Al_2O_3 and TiO_2 (e.g. α-Al_2O_3 and rutile–TiO_2). However, for modified nanostructured Al_2O_3-13wt.%TiO_2, plasma-reprocessing after the heat treatment yields the non-equilibrium phase of TiO_2. The disappearance of the rutile–TiO_2 phase indicates that melting has occurred during the plasma-reprocessing of the heat-treated powders. Thus, the presence of equilibrium α-Al_2O_3 and non-equilibrium anatase-TiO_2 may arise following the plasma-reprocessing from an air-quench that is rapid enough to form anatase–TiO_2. As shown in Fig. 3b, variation in the microstructure, ranging from dendritic-solidification structure to partially-molten (i.e. liquid phase sintered) morphology was observed for the modified nano-agglomerates. This inhomogeniety may be due to the variation in particle size and thermal history that individual particles experience during plasma reprocessing.

Fo plasma sprayed alumina–titania coatings, only α-Al_2O_3 and γ-Al_2O_3 phases were found and TiO_2 phases were absent. Since the solubility of TiO_2 in the equilibrium α-Al_2O_3 is negligible, Ti ions are likely to be in the γ-Al_2O_3 lattice as either an interstitial or substitutional defect. Formation of non-equilbrium γ-Al_2O_3 for plasma sprayed pure alumina coatings has been extensively reviewed by McPherson [14,15]. Recent XRD investigation by Kear et al. [24], suggests that the plasma sprayed Al_2O_3-13wt.%TiO_2 coatings contain non-equilibrium χ-$Al_2O_3 \cdot TiO_2$ phase in which Ti ions randomly occupy the Al^{3+} lattice sites in the γ-Al_2O_3 structure. The peak positions of XRD for χ-$Al_2O_3 \cdot TiO_2$ phase are identical to those of γ-Al_2O_3, however the relative intensity of peaks are different [24]. The formation of χ-$Al_2O_3 \cdot TiO_2$ phase must originate from rapid liquid-to-solid transformation, which is expected during the plasma spray process and provides reasonable explanation for the absence of Ti-containing phase. The non-equilibrium phase observed in this study can be identified as the χ-$Al_2O_3 \cdot TiO_2$ phase [24] by virtue of having the appropriate position and intensity of XRD peaks. Thus, the plasma sprayed nanostructured alumina–titania coatings consist of equilibrium α-Al_2O_3 and non-equilibrium χ-$Al_2O_3 \cdot TiO_2$ phase.

Table 3
Summary of visual inspection for plasma sprayed alumina–titania coatings from the bend test

CPSP	Commercial coating Metco-130	Nano-alumina–titania	Modified nano-alumina–titania[a]
300	Complete failure	Partial failure	Pass
325	Complete failure	Partial failure	Pass
350	–	–	Partial failure
410	Complete failure	–	–

[a] Modified with small amounts of other oxide additives.

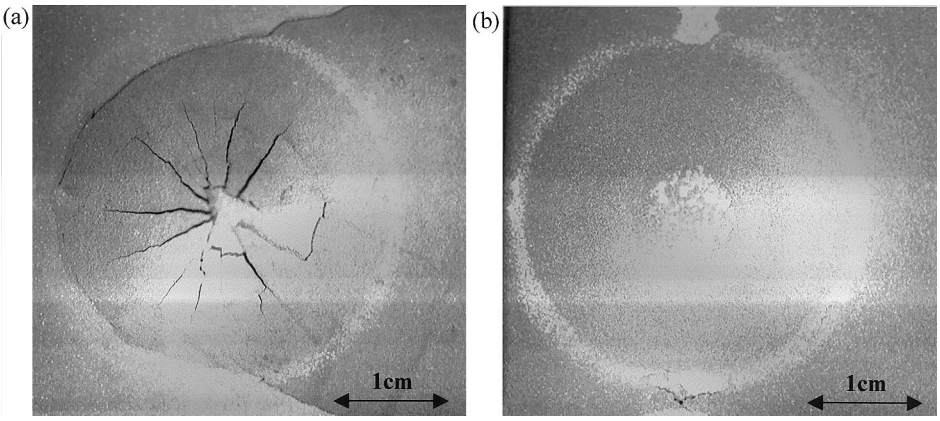

Fig. 12. Typical results observed for plasma sprayed (a) Metco-130 coatings and (b) nanostructured alumina–titania coatings after the cup tests. Significant cracking and spallation were observed for Metco-130 coatings, while minimum, localized spallation was observed for nanostructured alumina–titania coatings.

The presence of equilibrium α-Al_2O_3 in the plasma sprayed coatings has been examined by several investigators. Sokolova et al. [25] suggested that the presence of α-Al_2O_3 stems from unmelted α-Al_2O_3 feed particles and secondary α-Al_2O_3 formed by solid-state transformation as the substrate heats up. On the other hand, Zoltowski [26] concluded that the presence of α-Al_2O_3 was entirely due to the incorporation of unmelted feed particles. In the present work, the feed particles consisted of α-Al_2O_3. The results from XRD after plasma spray, as presented in Figs. 4 and 5, indicate that the amount of α-Al_2O_3 increases as the CPSP decreases. Since a decrease in the CPSP can be related to a decrease in plasma torch and/or particle temperature, the presence of α-Al_2O_3 in the alumina–titania coatings plasma sprayed from reconstituted nano-powder can be attributed to incomplete melting of the feed agglomerates. Quantitative image analysis shown in Fig. 7, has also demonstrated that the regions containing unmelted nano-Al_2O_3 particles, identified within the PM region in Fig. 6, increase with a decrease in CPSP. These results from XRD, microscopy and quantitative image analysis, consistently indicate that the presence of α-Al_2O_3 in the plasma sprayed alumina–titania coatings is a result of incomplete melting of the feed agglomerates. Based on this study, the phase transformation of Al_2O_3 as a function of CPSP can be summarized as shown in Table 4.

Variation in the amount of α- and γ-Al_2O_3 as a function of CPSP was not observed for Metco-130 coatings. Regardless of variation in the CPSP, Metco-130 coatings consisted primarily of γ-Al_2O_3, indicating that the commercial powders were completely melted and splat-quenched during plasma spray. The unchanging microstructure and mechanical properties of the Metco-130 with CPSP support this observation. Since Metco-130 powders and reconstituted powders differ significantly in microstructure (i.e. distribution of phases, grain size, porosity and particle size), physical processes involved in plasma spraying of powders with various microstructure are currently being investigated by a model based on computational fluid dynamics [27].

An investigation by Kear et al. [24] revealed that the grain size for the metastable χ-$Al_2O_3 \cdot TiO_2$ phase was in the nano-scale. Fig. 6c shows that the χ-$Al_2O_3 \cdot TiO_2$ phase corresponding to the splat-quenched FM region observed by electron microscopy in this study consists of nanostructured grains. In addition, Fig. 6d shows the nano/submicron size of the α-Al_2O_3 particles embedded in the alumina–titania coatings plasma sprayed from reconstituted nanostructured powders.

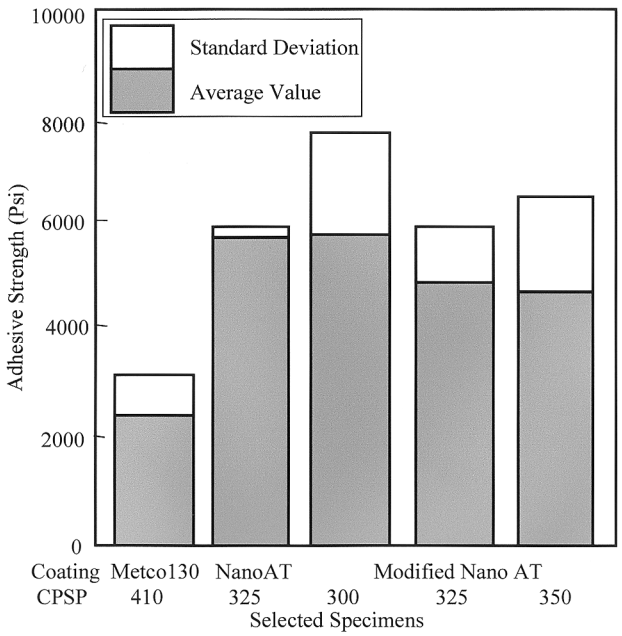

Fig. 13. Adhesive strength of selected alumina–titania coatings measured by modified direct-pull tests.

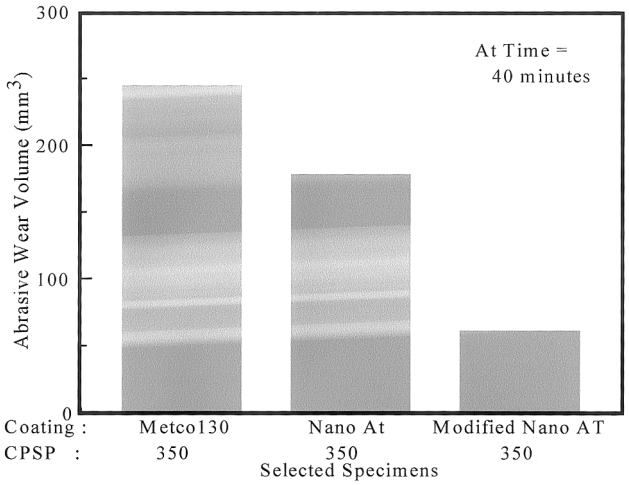

Fig. 14. Abrasive wear volume of plasma sprayed alumina–titania coatings at selected CPSP. The superior abrasive wear resistance, previously reported for nanostructured coatings [10], has been experimentally reproduced and verified in this study.

4.2. Mechanical properties and critical plasma spray parameter

Various properties, including porosity, hardness, indentation crack growth resistance, bend-test, cup-test, adhesive strength, abrasive and sliding wear resistance were evaluated for plasma sprayed alumina–titania coatings. The results, presented in Fig. 8 through 15, indicate that improvements in indentation crack growth resistance, resistance to cracking and spallation, adhesion strength, resistance to abrasive and sliding wear were observed for the nanostructured alumina–titania coatings, despite higher porosity and lower hardness. In addition, improvements in some properties were found at intermediate values of CPSP, for which partial melting of reconstituted agglomerates introduce sub-micron α-Al_2O_3. Further improvement in the modified Al_2O_3-13wt.%TiO_2 may be associated with chemistry as well as further reduction in grain size.

In this study, nano-coatings outperformed conventional coatings in cup and bend tests and the test results improved as the amount of PM microstructure increased and CPSP decreased as indicated in Figs. 11 and 12 and as reported in Table 3. Improvement in cup and bend test would be expected if the cracking perpendicular to the coatings/substrate interface occurs more easily than the spallation–debonding. Thus, the improved adhesive strength of nano-derived coatings would be expected to give improved cup and bend test results. Fig. 10 shows that the indentation crack growth resistance peaks at spray parameters of CPSP between 350 and 380. These results can be associated with a microstructural mixture having both FM and PM regions. It is further worth noting that the indentation cracking was almost exclusively parallel to the metal ceramic interface and many of the cracks are more than ten indentation diagonals long. It is likely that cracks extending so far from the indentation are influenced not only by the splat boundary weakness but also by residual stresses within the coating. Detailed studies on this issue are currently under way.

It is interesting to consider the relation between the improved mechanical properties and the observed microstructure. All the coatings deposited from the reconstituted nanostructured agglomerates had improved adhesive strength. Interestingly, the improvement in adhesive strength occurred regardless of the spray conditions or the fraction of the microstructure that was PM or even the presence of modifying elements as indicated in Fig. 13. During the adhesive strength test of nano-derived coatings, failures almost always occurred within the coating near the coating/substrate interface; thus the adhesive strength for the nano-derived coatings may be governed by the tensile strength of the nanostructured coatings. On the other

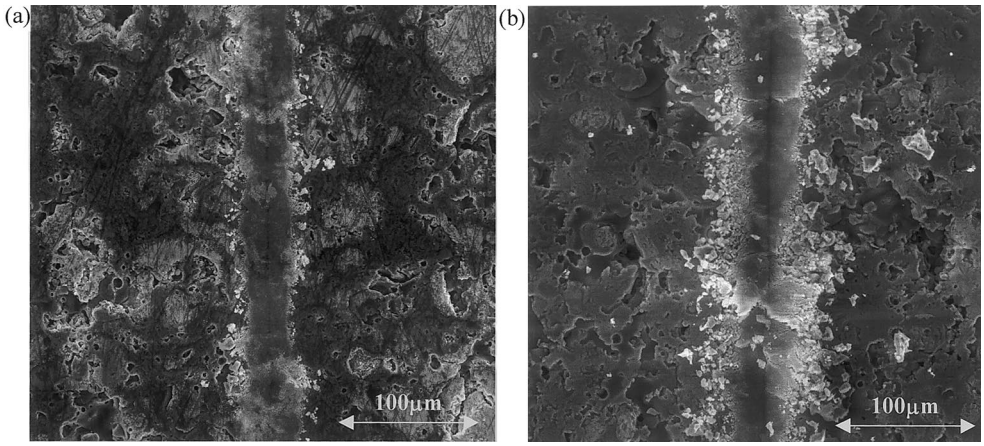

Fig. 15. Secondary electron images of wear tracks from 'scratch-tests' for (a) nanostructured and (b) Metco-130 coating. Wear track is observed to be larger with more material removal for Metco-130 coating.

Table 4
Summary of phase transformation possibilities for alumina–titania during the plasma spray process[a]

Starting powder	CPSE[b]	Constituent phases and transformations		
		Powder	During plasma spray	Coating
Commercial powder	All	α	Liquid	γ[c]
Reconstituted nanostructured powder	Low and intermediate	α	Solid	α
			Liquid	γ[c]
	High	α	Liquid	γ[c]

[a] The nanostructured coatings are produced by retaining the microstructure of the reconstituted nano-powders by partial melting at intermediate CPSP.
[b] Critical plasma spray parameter.
[c] Can be referred to as χ-Al_2O_3–TiO_2 phase [24].

hand, the Metco 130 coatings were the only coatings to show a significant fraction of failures at the ceramic to metal interface. The reason for the approximate doubling of the adhesive strength is not clear from the present study and is now being actively investigated with attention being paid to the higher purity chemistry and more uniform microstructure of the nano-materials.

5. Conclusions

Nanostructured alumina–titania coatings were produced by plasma spray of reconstituted nanostructured powders, using optimized processes, defined by a critical plasma spray parameter. Superior mechanical properties were achieved including indentation crack resistance, adhesion strength, spallation resistance against bend- and cup-test, abrasive wear resistance, sliding wear resistance. The superior properties are associated with coatings that have a retained nanostructure, especially with partial melting of the nanostructured powders.

Acknowledgements

The authors would like to thank Dr L. Kabacoff of Office of Naval Research (ONR), the program manager for this research and development effort under ONR Contract N00014-98-C-0010. Technical assistance of D. Mecklenburg at the University of Connecticut is also appreciated.

References

[1] B. Kear, L.E. Cross, J.E. Keem, R.W. Siegel, F.A. Spaepen, K.C. Taylor, E.L. Thomas, K.N. Tu, Research Opportunities for Materials with Ultrafine Microstructure, National Materials Advisory Board, National Academy Press, Washington, DC, 1989.
[2] H. Gleiter, Nanostruct. Mater. 1 (1992) 1.
[3] H. Hahn, Nanostruct. Mater. 2 (1993) 251.
[4] R.W. Siegel, Nanophase materials: synthesis, structure and properties, in: F.E. Fujita (Ed.), Physics of New Materials, Spinger, Heidelberg, 1992.
[5] R.S. Mishra, C.E. Lesher, A.K. Mukherjee, Mater. Sci. Forum 225–227 (1996) 617.
[6] R.W. Siegel, Mater. Sci. Forum 235–238 (1997) 851.
[7] K. Jia, T.E. Fischer, Wear 200 (1996) 206.
[8] K. Jia, T.E. Fischer, Wear 203–204 (1997) 310.
[9] L. Shaw, D. Goberman, R. Ren, M. Gell, S. Jiang, Y. Wang, T.D. Xiao, P.R. Strutt, Surf. Coat. Technol., 130 (2000), 1
[10] Y. Wang, S. Jiang, M. Wang, S. Wang, T.D. Xiao, P.R. Strutt, Wear, 37 (2000), 176
[11] M. Gell, J. Met., 46 (1994) 30.
[12] M. Gell, Mater. Sci. Eng. A204 (1995) 246.
[13] R. McPherson, J. Mater. Sci. 15 (1980) 3141.
[14] R. McPherson, J. Mater. Sci. 8 (1973) 851.
[15] R. McPherson, B.V. Shafer, Thin Solid Films 97 (1982) 201.
[16] I.A. Fisher, Int. Metall. Rev. 17 (1972) 117.
[17] T.R. Marlow, C.C. Koch, Mater. Sci. Forum 225–227 (1996) 595.
[18] L. Pawlowski, Surf. Coat. Technol. 31 (1987) 103.
[19] V. Wilms, H. Herman, Thin Solid Films 39 (1976) 251.
[20] S.Y. Semenov, B. Cetegen, unpublished research.
[21] L. Shaw, B. Barber, E.H. Jordan, M. Gell, Scr. Mater. 39 (1998) 1427.
[22] S.A. Saltykov, Streometric Metallography, second ed., Metallurgizdatnd, Moscow, 1958.
[23] Product Bulletin, Sulzer-Metco Corporation.
[24] B.H. Kear, Z. Kalman, R.K. Sadangi, G. Skandan, J. Colaizzi, W.E. Mayo, unpublished research.
[25] T.V. Sokolova, I.R. Kozolva, K. Derko, A.V. Kiiki, Izv. Akad. Nauk. S.S.S.R. Neorg. Mat. 9 (1968) 611.
[26] P. Zoltowski, Rev. Int. Hautes. Temper. Et Refract. 5 (1968) 253.
[27] I. Ahmed, T.L. Bergman, J. Thermal Spray Technol., 9 (2000) 240.